INTERNATIONAL JOURNAL FOR NUMERICAL METHODS IN FLUIDS
Int. J. Numer. Meth. Fluids 2009; **59**:519–533
Published online 16 June 2008 in Wiley InterScience (www.interscience.wiley.com). DOI: 10.1002/fld.1830

A two-component two-phase dissipative particle dynamics model

Anupam Tiwari and John Abraham*, †

School of Mechanical Engineering, Purdue University, West Lafayette, IN 47907, U.S.A.

SUMMARY

Dissipative particle dynamics (DPD)-based models for two-phase flows are attractive for simulating fluid flow at the sub-micron level. In this study, we extend a DPD-based two-phase model for a single-component fluid to a two-component fluid. The approach is similar to that employed in the DPD formulation for two immiscible liquids. Our approach allows us to control the density ratio of the liquid phase to the gas phase, which is represented independently by the two components, without changing the temperature of the liquid phase. To assess the accuracy of the model, we carry out simulations of Rayleigh–Taylor instability and compare the penetration rates of the spikes and bubbles formed during the simulations with prior results reported in the literature. We show that the results are in agreement with both experimental data and predictions from Youngs' model. We report these results for a broad range of Atwood numbers to illustrate the capability of the model. Copyright © 2008 John Wiley & Sons, Ltd.

Received 10 September 2007; Revised 20 March 2008; Accepted 27 March 2008

KEY WORDS: dissipative particle dynamics; molecular dynamics; particle methods; micro- and nano-scale flows; multiphase flows; interfacial instability

1. INTRODUCTION

With a growing interest in applications that involve the flow of fluid at sub-micron scales, it becomes important for us to understand the physics of fluids at these small scales. Applications where such flows are encountered include nano-scale machining [1], super-fine ink-jet printing [2] and drug-/gene-delivery to biological cells [3]. Features such as thermal fluctuations play an increasingly important role as the scales of the system decrease. Continuum formulations for fluid flow, such as the Navier–Stokes equations, cannot be used at such scales without modifications. Molecular dynamics (MD) [4], of course, is available as a computational tool at sub-micron scales, but computational cost precludes it as a tool for routine studies. Therefore, there is a need to develop computational methods that capture the physics at sub-micron scales and at the same time are computationally efficient. In this study, dissipative particle dynamics (DPD) [5, 6],

*Correspondence to: John Abraham, 500 Allison Road, West Lafayette, IN 47907-2014, U.S.A.
†E-mail: jabraham@ecn.purdue.edu

a particle-based mesoscopic computational method, is developed as a tool for studying a wide range of liquid–vapor density ratios in two-phase flows.

The formulation of DPD recognizes that not all details at the molecular level are required for capturing essential physics at the sub-micron level. Hence, coarse-graining can be carried out at the molecular level to retain only the essential physics. Dissipative 'particles' are then, conceptually, collections of a large number of molecules, though the precise correspondence between the two is not known *a priori*. Features such as thermal fluctuations at the sub-micron scale are captured by DPD [5, 7], and it further offers the flexibility of modeling complex fluids [8–11]. These features make it an attractive simulation tool for sub-micron fluid flows. For many of the sub-micron flows encountered, we need to model two phases with varying density ratios. For example, such models are required for the simulation of nanojets and nanobridges in the presence of an ambient gas. MD has recently been used [12] for simulations of nanobridges, and it has been shown that the physics of the breakup process at the nanolevel changes in the presence of an ambient gas compared with a vacuum.

Single-component two-phase DPD models have been developed in recent years [13–16]. These models work well in situations where the density ratio of the liquid phase to the vapor phase is high. This density ratio between two co-existing phases of the single-component fluid is determined by the temperature of the fluid. If low-density ratios are to be simulated, the temperature has to be increased. This may not be desirable from a numerical stability viewpoint, especially if the temperature is close to the critical point of the fluid. In this study, we extend a model for single-component two-phase flows to model systems that contain an additional component that could be either a liquid or a gas, i.e. it cannot undergo phase change. This allows us to change the density ratio by independently changing the properties of one component. Simulations can then be performed for a wide range of density ratios without changing the simulation temperature.

Since this study involves the development of a model to increase the range of density ratios that can be simulated using DPD, we need an appropriate test problem to evaluate the model. The Rayleigh–Taylor (R–T) instability is one such problem. It has been widely studied both numerically and experimentally. A two-component DPD model has been used in prior work for studying the R–T instability at a density ratio of 5 [17]. The distinguishing feature of our study relative to that study is that our study has two phases and two components. In our simulations of R–T instability at the sub-micron level, several values of density ratio and Atwood number are considered. The results are compared with experimental data and the predictions from Youngs' model [18, 19]. We study the R–T instability initiated by a single-mode perturbation in a two-dimensional box. Such simulations have been performed earlier using other mesoscopic methods, in addition to DPD [17]. For example, Nie *et al*. [20] and Tartakovsky and Meakin [21] have studied two-dimensional R–T instability using the lattice-Boltzmann method (LBM) and smoothed particle hydrodynamics (SPH), respectively. He *et al*. [22] have studied the single-mode R–T instability in three dimensions using LBM at a density ratio of 3, with the focus on the evolution of the interface in the non-linear growth stages. It is interesting to observe that potential flow theory [23] predicts that in single-mode R–T instability, the bubbles, i.e. the part of lighter fluid penetrating into the heavier fluid, move at a terminal velocity. However, recent numerical simulations [24] have shown that the bubbles in late-time R–T instability exhibit acceleration. This has been attributed to the presence of vortices in the bubble–spike interface, where spikes are the part of the heavier fluid penetrating into the lighter fluid. We observe a similar behavior in this study and the corresponding results are discussed.

This paper is organized as follows: In Section 2, we describe the DPD two-phase model and the extension of the model to include two components. In Section 3, we describe the problem setup

DOI: 10.1002/fld

for R–T simulations. In Section 4, we present the results from the different simulations performed in this study. We conclude the paper with summary and conclusion in Section 5.

2. THE DPD TWO-PHASE MODEL

In this section, we provide a brief overview of the DPD two-phase model. A detailed description of the model can be found in Reference [16]. The evolution of a DPD particle i of unit mass is followed by solving Newton's laws of motion, i.e.

$$\begin{aligned} \frac{\mathrm{d}\mathbf{r}_i}{\mathrm{d}t} &= \mathbf{v}_i \\ \frac{\mathrm{d}\mathbf{v}_i}{\mathrm{d}t} &= \mathbf{f}_i \end{aligned} \tag{1}$$

where $\mathbf{r}_i, \mathbf{v}_i$ and $\mathbf{f}_i$ denote the position, velocity and force vectors, respectively. The contribution to $\mathbf{f}_i$ arises from interparticle forces $\mathbf{F}_{ij}$ between the DPD particles. To model this, the interaction force is split into three components, namely the dissipative, random and conservative forces. The dissipative force $\mathbf{F}_{ij}^{\mathrm{D}}$ is responsible for the viscous effects in the DPD system and acts to reduce the relative velocity between any two particles in an interacting pair. The random force $\mathbf{F}_{ij}^{\mathrm{R}}$ is included to account for the degrees of freedom lost in coarse-graining. At the molecular level there are many collisions that take place between the actual atoms/molecules. However, when a group of atoms/molecules is represented by a DPD particle, there is a reduction in the number of collisions. This loss is accounted for by including the random force. The random force tends to heat up the DPD system as it supplies energy to the two interacting particles. This is in contrast to the effect of the dissipative force that tends to cool down the DPD system. A balance condition between these two forces is required for simulating the isothermal systems that we consider in this study. This balance condition is achieved by applying the fluctuation–dissipation theorem [6] to choose the parameters for the force models. The dissipative and random forces are responsible for the hydrodynamic behavior of the DPD system. The third component of the interparticle force of interaction is the conservative force $\mathbf{F}_{ij}^{\mathrm{C}}$, which accounts for the configurational energy of the DPD system; it is responsible for the thermodynamic behavior of the DPD system.

The functional forms of the forces between particles i and j are given by [6]

$$\begin{aligned} \mathbf{F}_{ij}^{\mathrm{D}} &= -\gamma\omega^{\mathrm{D}}(r_{ij})(\mathbf{e}_{ij}\cdot\mathbf{v}_{ij})\mathbf{e}_{ij} \\ \mathbf{F}_{ij}^{\mathrm{R}} &= \sigma\omega^{\mathrm{R}}(r_{ij})\xi_{ij}\mathbf{e}_{ij} \quad \text{and} \\ \mathbf{F}_{ij}^{\mathrm{C}} &= -\frac{\partial\psi(r_{ij})}{\partial r_{ij}}\mathbf{e}_{ij} \end{aligned} \tag{2}$$

Here, $\mathbf{e}_{ij}$ is a unit vector given by $\mathbf{e}_{ij} = \mathbf{r}_{ij}/|\mathbf{r}_{ij}|$, where $\mathbf{r}_{ij} = \mathbf{r}_i - \mathbf{r}_j$, $\mathbf{v}_{ij} = \mathbf{v}_i - \mathbf{v}_j$, γ is the amplitude of the dissipative force, σ is the amplitude of random force, ω^{D} and ω^{R} are the weight functions for the dissipative and random forces, respectively, and ψ is the free energy per particle. DPD is a short-ranged method, i.e. each particle can interact only with particles that are within a certain cut-off radius from it. This feature is attractive from a computational viewpoint since it restricts the number of particle interactions that have to be accounted for. The cut-off radius is modeled in

DOI: 10.1002/fld

the DPD system through the weight functions that go to zero beyond the radius. The term ξ_{ij} in Equation (2) is a random variable that has zero mean, unit variance and is uncorrelated in time. It follows Gaussian statistics and has the following properties:

$$\begin{aligned} \langle \xi_{ij}(t) \rangle &= 0 \\ \langle \xi_{ij}(t) \xi_{kl}(t') \rangle &= (\delta_{ik}\delta_{jl} + \delta_{il}\delta_{jk})\delta(t-t') \end{aligned} \tag{3}$$

Additional details about the force components and the choice of parameters can be found in [7].

As mentioned earlier, the fluctuation–dissipation theorem is applied to the DPD system to give a balance condition between the dissipative and random forces. It gives the following relationship between their amplitudes and weight functions [6]:

$$\omega^{\mathrm{D}}(r) = [\omega^{\mathrm{R}}(r)]^2, \quad \sigma^2 = 2\gamma k_{\mathrm{B}} T \tag{4}$$

In this study, we have chosen a commonly adopted functional form for the weight functions for dissipative and random forces, which depends on the interparticle separation r and the cut-off radius r_{c}, and is given by

$$\omega^{\mathrm{D}}(r) = [\omega^{\mathrm{R}}(r)]^2 = \begin{cases} \left(1 - \dfrac{r}{r_{\mathrm{c}}}\right)^2 & (r < r_{\mathrm{c}}) \\ 0 & (r \geqslant r_{\mathrm{c}}) \end{cases} \tag{5}$$

The DPD equations of motion are integrated using the following modified-Verlet scheme of Reference [7]:

$$\begin{aligned} \mathbf{r}_i(t+\delta t) &= \mathbf{r}_i(t) + \delta t \mathbf{v}_i(t) + \tfrac{1}{2}(\delta t)^2 \mathbf{f}_i(t) \\ \tilde{\mathbf{v}}_i(t+\delta t) &= \mathbf{v}_i(t) + \lambda \delta t \mathbf{f}_i(t) \\ \mathbf{f}_i(t+\delta t) &= \mathbf{f}_i(\mathbf{r}(t+\delta t), \tilde{\mathbf{v}}(t+\delta t)) \\ \mathbf{v}_i(t+\delta t) &= \mathbf{v}_i(t) + \tfrac{1}{2}\delta t (\mathbf{f}_i(t) + \mathbf{f}_i(t+\delta t)) \end{aligned} \tag{6}$$

where $\mathbf{r}, \mathbf{v}$ and $\mathbf{f}$ denote the position, velocity and force vectors, respectively, t denotes the time, i denotes a particle tag and λ denotes an empirical parameter. The quantity $\tilde{\mathbf{v}}$ is a guessed value of the velocity. This guess is necessary because the force depends on velocity as seen from the third line in Equation (6).

To model two-phase flows, the conservative force has to be modified to incorporate the surface tension force and bring about phase segregation. At the molecular level, the interaction between two atoms/molecules is attractive when they are far apart compared with the molecular diameter. This interaction between the atoms/molecules becomes repulsive when they approach each other and the separation is close to the molecular diameter. These features naturally give rise to the properties of phase segregation and surface tension. From a modeling perspective, this feature can be captured by choosing an appropriate potential such as the Lennard-Jones potential [4]. However, at the mesolevel we do not use such a potential and hence modeling is required to capture these features.

There are several models in the literature for modeling liquid–vapor systems with DPD [13–16]. In our two-phase model, the conservative force that gives rise to phase segregation and surface

DOI: 10.1002/fld

tension is modeled by employing mean-field theory [25] as follows:

$$\mathbf{F}^{\mathrm{C}} = -\nabla\psi_{\text{non-ideal}} + \kappa\nabla\nabla^2\rho \tag{7}$$

where $\psi_{\text{non-ideal}}$ denotes the non-ideal part of the free energy, κ denotes a model parameter that controls the strength of surface tension and is related to the second moment of the attractive component of interaction potential between atoms/molecules and ρ is the density. This approach has been employed in other mesoscopic numerical methods [26–28]. In Equation (7) the first term is responsible for phase segregation and the second term is responsible for surface tension. The free energy is derived from an equation of state with a van der Waals (VW) loop. In this study, we use a VW equation of state given by

$$p = \frac{\rho k_{\mathrm{B}} T}{1 - b\rho} - a\rho^2 \tag{8}$$

where p denotes the pressure, ρ denotes the density, k_{B} denotes the Boltzmann constant, T denotes the temperature and a and b are parameters for the equation of state, which are related to the zeroth moment of the attractive part of interaction potential and exclusion volume effects, respectively. We will now provide the final set of equations that specify this model. Additional details about the model can be found in Reference [16].

We see from Equation (7) that the surface tension term depends on the gradients of density. The density ρ in the vicinity of particle i is calculated using the following expression:

$$\rho_i = \sum_{j=1}^{N} w(r_{ij}) \tag{9}$$

where w denotes the normalized weight function, j denotes a particle tag, r denotes the separation and N denotes the total number of particles. We note that the form of weight function given by Equation (5), which is employed in the calculation of dissipative and random forces, would not suffice for Equation (9) as we need to calculate the third derivative of density in Equation (7). Therefore, we choose the Lucy weight function [29], used extensively in other particle-based methods [30, 31], which for the two-dimensional case is given by

$$w(r, r_{\mathrm{c}}) = \begin{cases} \dfrac{5}{\pi r_{\mathrm{c}}^2}\left(1 + \dfrac{3r}{r_{\mathrm{c}}}\right)\left(1 - \dfrac{r}{r_{\mathrm{c}}}\right)^3 & \text{if } r < r_{\mathrm{c}} \\ 0 & \text{if } r > r_{\mathrm{c}} \end{cases} \tag{10}$$

where r denotes the interparticle separation and r_{c} denotes the cut-off radius. Using the definition of density in Equation (9) and substituting the free energy obtained from Equation (8) into Equation (7), the final form of the interparticle conservative force is obtained as

$$\mathbf{F}_{ij}^{\mathrm{C}} = \left[-\left\{ \left(\frac{bk_{\mathrm{B}}T}{1 - b\rho_i} - a \right) + \left(\frac{bk_{\mathrm{B}}T}{1 - b\rho_j} - a \right) \right\} w_{ij}^{(1)} + \kappa w_{ij}^{(3)} \right] \mathbf{e}_{ij} \tag{11}$$

where $w_{ij}^{(1)}$ and $w_{ij}^{(3)}$ denote the first and third derivatives of the weight function in Equation (10) with respect to the interparticle separation. The parameters that are required for specifying the interparticle conservative force are $a, b, \kappa, r_{\mathrm{c}}$ and $k_{\mathrm{B}}T$.

DOI: 10.1002/fld

Different density ratios can be obtained in the model by changing the temperature, i.e. the temperature has to be increased to obtain lower density ratio while decreased for higher density ratio. There are two potential difficulties when doing this. The first is that as lower density ratios are specified, the temperature will increase toward the critical value. This model based on the mean-field theory is not applicable in the vicinity of the critical point. This poses a limit on the lower value of density ratio. The second is that as we change the temperature, the properties of the fluid also change; for example, with increasing temperature, the viscosity will decrease. These factors have the net effect of limiting the model to studies of single-component fluids at high-density ratios. If we can formulate a method that allows us to change the density ratio without changing the temperature, it would be an attractive tool for simulating two-phase systems using DPD. Groot and Warren [7] have given a theory for simulating liquid–liquid systems with DPD. They have shown that appropriately chosen parameters for the interparticle conservative force can be used for simulating immiscible liquids. We use a fundamentally similar approach to simulate systems in which multiple components are present. One of the components is a fluid that follows a VW equation of state and will give rise to liquid and vapor phases, while the other component could be either a liquid or a gas, i.e. it cannot change phase. This component is modeled using the form of the conservative force used in DPD [7]. We now discuss how this is done.

The conservative force $\mathbf{F}_{ij}^{\mathrm{C}}$ between particles i and j in the formulation of DPD in Reference [7] is given by

$$\mathbf{F}_{ij}^{\mathrm{C}} = a_{ij}\left(1-\frac{r_{ij}}{r_{\mathrm{c}}}\right)\mathbf{e}_{ij} \tag{12}$$

where a_{ij} is the repulsion parameter, r is the interparticle separation, r_{c} is the cut-off radius and $\mathbf{e}_{ij}$ is the unit vector joining particles i and j. Let us call this fluid the Groot–Warren (GW) fluid. This GW fluid can co-exist with a fluid that has a conservative force defined by Equation (11). Let us refer to the fluid defined by Equation (11) as the VW fluid. As we know, the VW fluid follows a VW equation of state and depending on the simulated state point it will contain liquid and vapor particles. Therefore, three types of interactions are possible in a domain that consists of GW and VW fluids. These interactions are between the particles of GW fluid denoted by GW–GW, the interactions between particles of VW fluid denoted by VW–VW and the interactions between particles from GW and VW fluids denoted by GW–VW. The conservative components of GW–GW and VW–VW interactions can be modeled using Equations (12) and (11), respectively. To model the conservative components of GW–VW interactions, we can choose Equation (12) and specify a value for the parameter a_{ij}, which is more than the value it has for GW–GW interactions. This will lead to repulsion between the GW and VW fluids.

With this model it is possible to study two-component systems for a wide range of density ratios. Unlike the previous models, we do not need to change the temperature for simulations at different density ratios. This allows us to independently study the influence of density ratio without affecting other properties of fluids. Next, we will apply this method to a test problem.

3. PROBLEM SETUP

As mentioned earlier, the R–T instability has been studied with a wide range of numerical methods, including MD, DPD, LBM and SPH [17, 20–22, 32, 33]. The instability develops when a heavier fluid rests on top of a lighter fluid in the presence of a gravitational field. When this is done,

DOI: 10.1002/fld

perturbations at the interface tend to grow with time and the heavier fluid penetrates the lighter fluid. The parts of the heavier fluid entering the lighter fluid are called spikes. The parts of the lighter fluid penetrating the heavier fluid are called bubbles. Our objective here is not to provide new insights into R–T instability, but only to use it as a test problem for our model. Before we do this, we will briefly review the findings from the MD and DPD studies.

Dzwinel *et al*. [32] performed two-dimensional MD simulations and found that the dynamics of bubbles and spikes are the same at the molecular and macrolevels. They also showed that, in agreement with macroscopic observations, the growth rate coefficient for bubbles is independent of the Atwood number. The Atwood number A is a parameter of key interest in R–T instability simulations as it can be related to the mixing rate. It is defined as

$$A = \frac{\rho_l - \rho_v}{\rho_l + \rho_v} \tag{13}$$

where ρ_l and ρ_v are the densities of the heavier and lighter fluids, respectively. Kadau *et al*. [33] performed large-scale MD simulations using up to 100 million particles and showed that the mixing behavior at the molecular level is in agreement with the behavior at the macrolevel. They found good quantitative agreement between the values of growth coefficients for bubbles and spikes determined from MD simulations, experimental data and Youngs' model [18, 19]. Prior simulations [17] of R–T instability using the GW model were at a density ratio of 5, which corresponds to an A of about 0.67. In this study, we have performed simulations for values of A in the range of 0.35–1. Note that A of 1 corresponds to R–T simulations in vacuum. For the cases in which an ambient fluid is present, we have performed simulations for density ratios ranging from 2.1 to 17.2.

The computational domain for the study is shown in Figure 1. The simulations are carried out in a slab, i.e. they are two dimensional. Recall that our objective is to assess the model. Hence, two-dimensional simulations are adequate. It is, however, interesting to note that Kadau *et al*. [33] carried out their MD simulations in a slab as well as in three-dimensional domains, and no

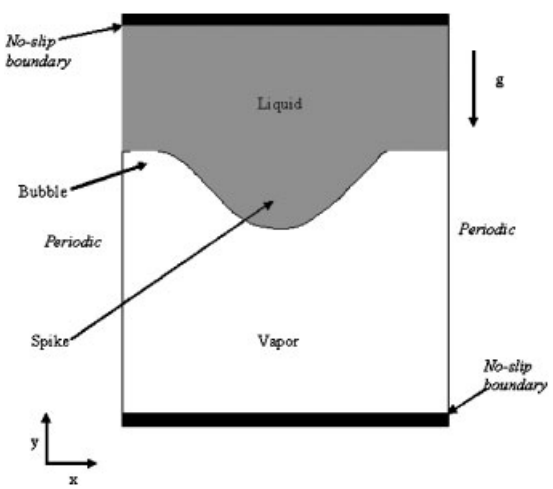

Figure 1. Computational setup for Rayleigh–Taylor instability simulations.

DOI: 10.1002/fld

noticeable differences in results were reported. We will also be reporting on only single-bubble dynamics and will not be studying the interaction of multiple bubbles. Again, this is reasonable given the limited objective of our study.

We apply periodic boundary conditions for the left- and right-hand sides of the computational domain. No-slip boundary conditions are applied to the bottom and top of the computational domain. This requires special treatment for the two-phase two-component model, and this treatment will be described now. When we look at the form of the interparticle conservative force for a VW fluid as given by Equation (11), we see that there is a dependence on density as well as derivatives of weight functions. This dependence makes it important for us to apply the boundary condition in a manner such that the density calculation can be done accurately. In this study, for implementing the no-slip walls, we model the density of wall particles to be equal to the density of the surrounding fluid. The thickness of the wall is chosen to be equal to the cut-off radius because there is no interaction between particles beyond this range. When particles try to penetrate the boundary, they are re-introduced into the computational domain according to the bounce-back rule [34]. The particles in the interfacial region are given an initial sinusoidal perturbation to initiate the instability. In DPD, thermal fluctuations are an intrinsic part of the system and the instability can be initiated just by the thermal fluctuations. This has been observed in MD simulations [33] and DPD simulations [17]. We, however, apply an explicit perturbation because it accelerates the initiation of the instability.

4. SIMULATION RESULTS

In this section we present the results from simulations that were performed to assess the two-phase two-component model for a range of density ratios. Our focus is on lower density ratios, since this is the range where existing two-phase models encounter difficulties. The simulation parameters used for this study are given in Table I. The penetration h of bubbles and spikes for late-time mixing can be expressed by the general formula [18, 35, 36]

$$h_{\mathrm{b,s}} = \alpha_{\mathrm{b,s}} A g t^2 \tag{14}$$

where α is a constant for a given Atwood number A, g is the acceleration due to gravity, t is the time and the subscripts b and s refer to bubbles and spikes, respectively. The reason for using this equation for comparing the single-mode R–T results presented in this paper is discussed below. In this study we have performed simulations at $A=1$ and seven additional values of the Atwood number given in Table II. For these seven values, we use both the VW and the GW fluids, but, for the simulation at $A=1$, we use only the VW fluid. The densities of the GW fluid for the simulations in Table II are 2, 3, 4, 6, 8, 12 and 16. This corresponds to density ratios of about 17.2, 10.8, 8.1, 5.4, 4.1, 2.8 and 2.1, respectively. The parameter α, for spikes, has been shown in prior studies to increase with increasing values of A. The values of the repulsion parameter a in Equation (12) for the conservative force between the particles in GW–GW and GW–VW pairs are given in Table II. It is important to note that the parameter $a_{\mathrm{GW-VW}}$ controls the miscibility between the GW and VW fluids. An increasing value of this parameter reduces the miscibility between the two fluids. This effect is shown in Figure 2, which shows results for a simulation performed at $A=0.35$ using the parameters in Table I. The top row shows the VW fluid, while the bottom row shows the GW fluid. The snapshots are taken at the same DPD time of 200 units.

DOI: 10.1002/fld

Table I. Simulation parameters for Rayleigh–Taylor study.

Parameter	Equation in which the parameter appears	Value in DPD units
$k_B T$	(4, 11)	0.7
a (van der Waals parameter)	(11)	1.0×10^{-1}
b (van der Waals parameter)	(11)	2.5×10^{-2}
σ	(2)	2.0
κ	(11)	5.0×10^{-3}
Time step δt	(6)	1.0×10^{-2}
r_c	(5, 10, 12)	1.11
g	—	1.2×10^{-2}

Table II. Repulsion parameters for conservative force between different types of particles.

Atwood number (A)	GW–GW pair	GW–VW pair
0.35	3.10×10^{-3}	2.53×10^{-1}
0.47	5.60×10^{-3}	1.12×10^{-1}
0.61	1.25×10^{-2}	2.50×10^{-1}
0.69	2.22×10^{-2}	4.44×10^{-1}
0.78	5.00×10^{-2}	5.00×10^{-1}
0.83	8.90×10^{-2}	5.00×10^{-1}
0.89	2.00×10^{-1}	5.00×10^{-1}

We see that as the repulsion parameter between the two fluids is increased, there is lesser mixing between the two. The ability to choose the repulsion parameter provides us with the ability to control the miscibility between the two fluids.

Figure 3 shows snapshots during the development of instability for an A value of 0.61. We have shown only the particles of the VW fluid for clarity. We see that there is a slow growth of the instability until about $t = 80$, i.e. Figure 3(c). After this there is a rapid growth of the instability. This late-time behavior is consistent with Equation (14). The density ratio of the heavier fluid to the lighter fluid has an impact on the penetration rate of bubbles and spikes. This can be seen in Figure 4, which shows the snapshots of the fluid at the same DPD time of $t = 120$ for simulations at different values of A. We show only the VW fluid for clarity. We see that with decreasing values of A, i.e. with decreasing density ratio, the penetration decreases as expected since there is a denser mass of fluid in front of the moving spikes. It is also seen that for the case with the larger value of A, the spikes reach the bottom of the computational domain faster.

Potential flow theory [23] predicts a terminal velocity for the bubble in single-mode R–T instability. However, the presence of vortices in the bubble–spike interface, for the case of single-bubble cases, has been shown [24] to produce acceleration of the bubble. This is because the vortices cause a reduction in the drag force on the bubbles and spikes. Tartakovsky and Meakin [21] have used SPH to simulate single-mode R–T instability and have also observed a quadratic dependence of the instability amplitude on time. In the DPD simulations presented in this study,

DOI: 10.1002/fld

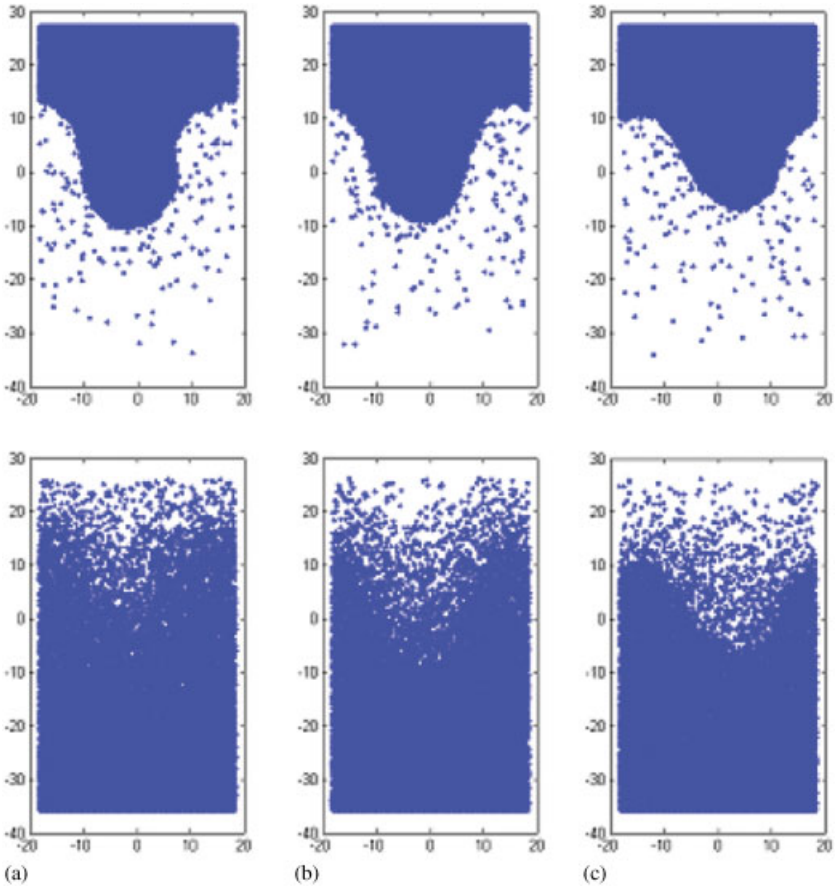

Figure 2. Snapshots of the computational domain for Rayleigh–Taylor simulations at $A = 0.35$ for different values of repulsion parameter between the VW (top row) and GW fluids (bottom row) at a DPD time of 200 units.

we observe vortices in the bubble–spike interface. Figure 5 shows the vector plot from one such simulation, which was performed at $A = 0.35$. An ensemble-averaging has been performed over 15 instances to remove the noise present in results because of thermal fluctuations. We see two vortices in the simulation domain, which are centered approximately at $(-5, -10)$ and $(12, -12)$. Such vortices have been shown in the study by Ramaprabhu *et al*. [24] to induce acceleration to the motion of bubbles. Hence, we have chosen Equation (14) to describe the motion of bubbles and spikes and have compared DPD simulation results in this study with the results presented in a prior study.

Figure 6 shows the penetration of bubbles and spikes as a function of the square of time for the simulations at $A = 0.35, 0.61$ and 1. Several observations can be made. In all cases, the penetration of spikes is faster than the penetration of bubbles. The rate of penetration of spikes increases with increasing values of A, while the rate of penetration of bubbles has a smaller dependence on A. These observations are in agreement with the experimental data available in the literature [18].

DOI: 10.1002/fld

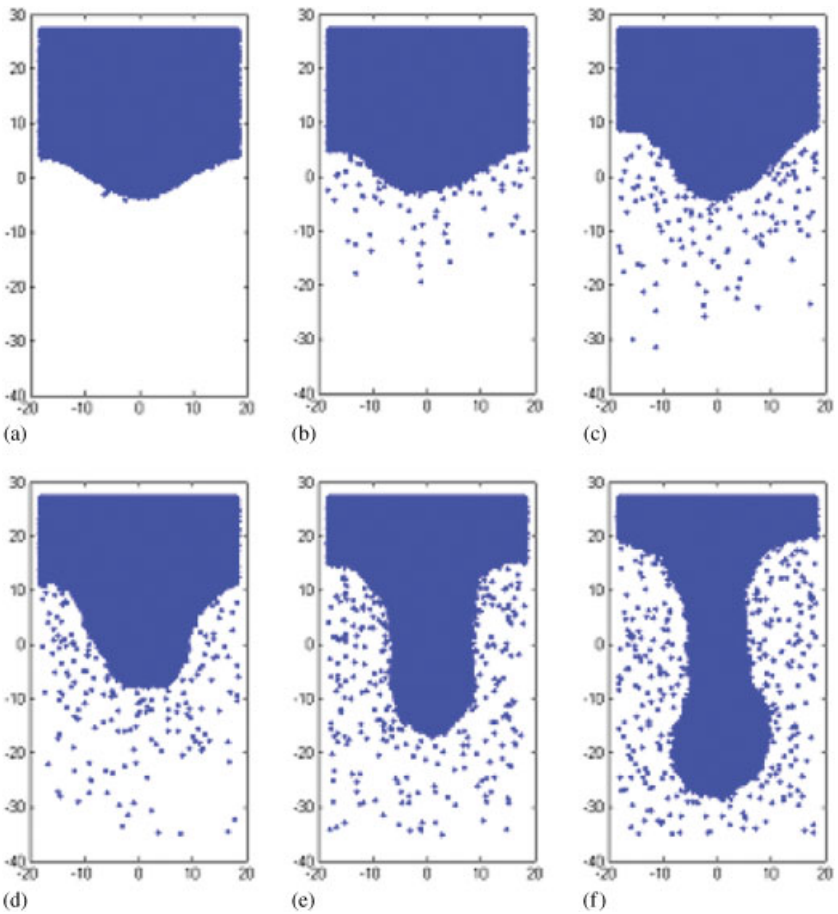

Figure 3. Snapshots of the computational domain for Rayleigh–Taylor simulation performed for $A=0.61$, at (a) $t=1$, (b) $t=40$, (c) $t=80$, (d) $t=120$, (e) $t=160$ and (f) $t=200$.

The motion of bubbles and spikes is governed by a balance between inertia, buoyancy and drag forces [37]. The displacement of fluid, which is being penetrated into, and the mixing render a complicated nature to the process. This also tends to reduce the density ratio between the two fluids [18]. Youngs [18, 19] has developed a phenomenological model for predicting the parameter α appearing in Equation (14) as a function of A. In the model, it is assumed that the mixing process does not impact the density ratio between the fluids. The model introduced density-dependent drag coefficients for bubbles and spikes and couples their length scales [18]. The unknown parameter in Youngs' model is the drag coefficient, which is required for determining the value of α for bubbles and spikes. A value of 3.67 for the drag coefficient has been shown to give a difference of about 20% when compared with experimental data [18]. A comparison of the values of this parameter α from Youngs' prediction, with drag coefficient $C=3.67$, and those obtained from our DPD simulations is provided in Figure 7. The error bars in the computational results are estimated by accounting for the uncertainty in determining the interface due to thermal fluctuations

DOI: 10.1002/fld

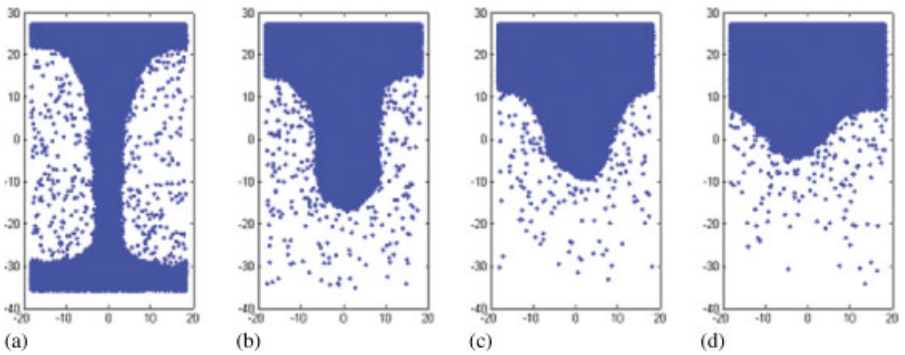

Figure 4. Snapshots of the computational domain at time $t = 120$ for simulations at the Atwood numbers of (a) 1, (b) 0.61, (c) 0.47 and (d) 0.35. Pictures show VW fluid, GW fluid present in (b), (c) and has not been shown for clarity in (d).

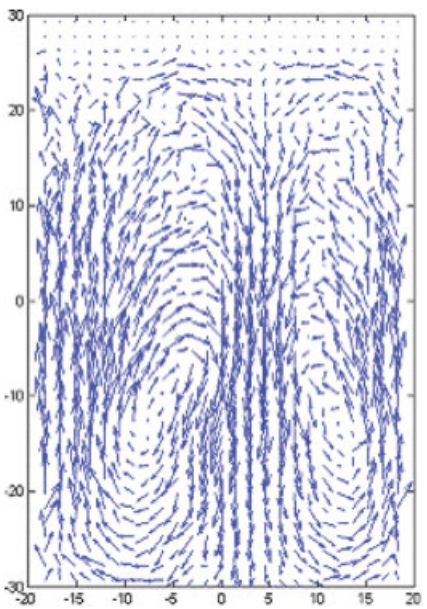

Figure 5. Vector plot of the R–T-simulation domain showing the presence of vortices in the bubble–spike interface.

and employing Equation (14). In this figure, we also show the experimental data obtained by Dimonte [18]. The results presented here are also in agreement with the MD simulations results of Kadau *et al*. [33]. Their simulations used thin slabs as well as full three-dimensional domains. They did not find a statistical difference between the two. We see from Figure 7 that the values of α for bubbles have a weak dependence on A, but they have a strong dependence for spikes. The value of α is found to increase with increasing A. The motion of spikes is resisted by

DOI: 10.1002/fld

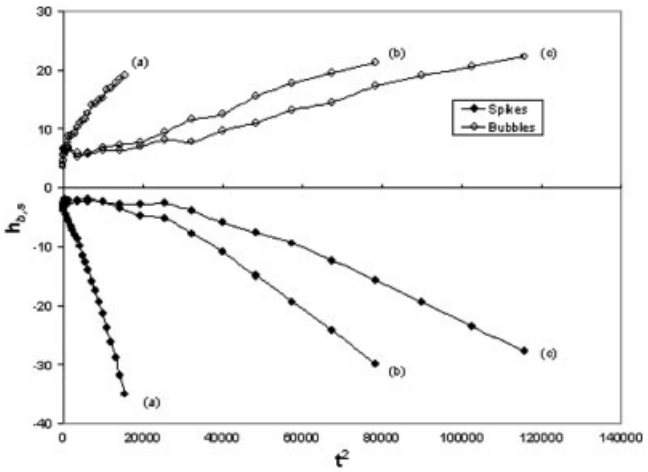

Figure 6. Penetration of bubbles and spikes as a function of square of time for Atwood numbers of (a) 1, (b) 0.61 and (c) 0.35. Values are in DPD units.

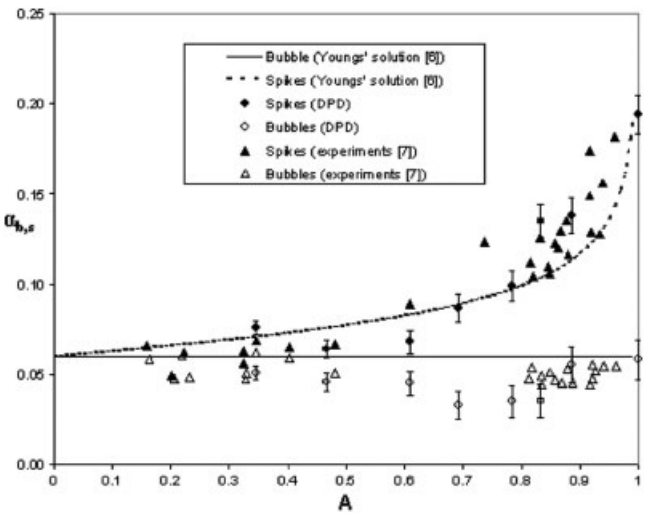

Figure 7. Comparison of results from DPD simulations with the phenomenological model by Youngs and experimental data from Reference [18].

low-density gas/vapor, while the motion of bubbles is resisted by high-density liquid. Hence, with increasing values of A, spikes penetrate with greater momentum, but bubbles penetrate at almost the same rate. Based on the simulations that we have performed, thermal fluctuations do not seem to have an influence on the late-time behavior of the instability, and the observations are in agreement with the macroscopic case. This conclusion is also consistent with the findings from MD simulations.

DOI: 10.1002/fld

5. SUMMARY AND CONCLUSIONS

In this study, we have extended a recently proposed DPD model for single-component two-phase flows to include an additional component. The additional component and its interaction with the two-phase fluid are modeled using the form of conservative force proposed by Groot and Warren [7]. The repulsion parameter for the conservative force of interaction between GW and VW fluid particles is chosen to have a value that is more than its value for the interaction between the GW and GW fluid particles. This allows us to control the miscibility of the GW fluid in the DPD two-phase (VW) fluid. Existing DPD-based two-phase models have a limitation of not being able to simulate systems at low values of liquid-to-vapor density ratios. The two-component two-phase model presented in this study has been developed to simulate systems at a wide range of density ratios ranging from very high to very low values. To evaluate the model, we have employed it to simulate single-mode Rayleigh–Taylor (R–T) instability. The R–T instability has been extensively studied in the literature using various experimental and numerical methods. The presence of vortices in the bubble–spike interfacial region leads to a reduction in the drag force on bubbles and spikes. This leads to a t^2 dependence to the late-time penetration rate of bubbles and spikes. This behavior has also been observed in prior computational studies [21, 24].

It is encouraging that the model reproduces expected trends in the behavior of bubbles and spikes. Simulations have been performed for density ratios ranging from 2.1 to 17.2 and also for the limiting case where the vapor phase has vanishingly low density. The spikes are found to penetrate faster than the bubbles. It is also found that the parameter α appearing in Equation (14) for the penetration of spikes and bubbles has a value that increases with increasing Atwood number (A) for the spikes. For the case of bubbles, it has been found that this parameter has a smaller dependence on the changing values of the Atwood number. We have shown that these observations are in agreement with experimental results and the predictions from Youngs' model. In agreement with MD simulations, we see that the late-time behavior of R–T instability is not influenced by the presence of thermal fluctuations. These simulations show the ability of the new model to capture the physics over a wide range of density ratios.

REFERENCES

1. Ye YY, Biswas R, Morris JR, Bastawros A, Chandra A. Molecular dynamics simulation of nanoscale machining of copper. *Nanotechnology* 2003; **14**:390–396.
2. Murata K, Matsumoto J, Tezuka A, Matsuba Y, Yokoyama H. Super-fine ink-jet printing: toward the minimal manufacturing system. *Microsystem Technologies* 2005; **12**:2–7.
3. Furth PA. Gene transfer by biolistic process. *Molecular Biotechnology* 1997; **7**:139–143.
4. Allen MP, Tildesley DJ. *Computer Simulation of Liquids*. Oxford Science Publications: Oxford, 1987.
5. Hoogerbrugge PJ, Koelman JMVA. Simulating microscopic hydrodynamics phenomena with dissipative particle dynamics. *Europhysics Letters* 1992; **19**:155–160.
6. Espanol P, Warren PB. Statistical mechanics of dissipative particle dynamics. *Europhysics Letters* 1995; **30**: 191–196.
7. Groot RD, Warren PB. Dissipative particle dynamics: bridging the gap between atomistic and mesoscopic simulation. *Journal of Chemical Physics* 1997; **107**:4423–4435.
8. Symeonidis V, Karniadakis GV, Caswell B. Dissipative particle dynamics simulations of polymer chains: scaling laws and shearing response compared to DNA experiments. *Physical Review Letters* 2005; **95**:076001.
9. Boek ES, Coveney PV, Lekkerkerker HNW. Simulating the rheology of dense colloidal suspensions using dissipative particle dynamics. *Physical Review E* 1997; **55**:3124–3133.
10. Fan X, Thien N-P, Yong NT, Wu X, Xu D. Microchannel flow of a macromolecular suspension. *Physics of Fluids* 2003; **15**:11–21.

DOI: 10.1002/fld

11. Palma PD, Valentini P, Napolitano M. Dissipative particle dynamics simulation of a colloidal micropump. *Physics of Fluids* 2006; **18**:027103.
12. Kang W, Landman U. Universality crossover of the pinch-off shape profiles of collapsing liquid nanobridges in vacuum and gaseous environments. *Physical Review Letters* 2007; **98**:064504.
13. Pagonabarraga I, Frenkel D. Dissipative particle dynamics for interacting systems. *Journal of Chemical Physics* 2001; **115**:5015–5026.
14. Warren PB. Vapor–liquid coexistence in many-body dissipative particle dynamics. *Physical Review E* 2003; **68**:066702.
15. Liu M, Meakin P, Huang H. Dissipative particle dynamics with attractive and repulsive particle–particle interactions. *Physics of Fluids* 2006; **18**:017101.
16. Tiwari A, Abraham J. Dissipative-particle-dynamics model for two-phase flows. *Physical Review E* 2006; **74**:056701.
17. Dzwinel W, Yuen DA. Mixing driven by Rayleigh–Taylor instability in the mesoscale modeled with dissipative particle dynamics. *International Journal of Modern Physics C* 2001; **12**:91–118.
18. Dimonte G. Spanwise homogeneous buoyancy-drag model for Rayleigh–Taylor mixing and experimental evaluation. *Physics of Plasmas* 2000; **7**:2255–2269.
19. Hanson JC, Rosen PA, Goldsack TJ, Oades K, Fieldhouse P, Cowperthaite N, Youngs DL, Mawhinney N, Baxter AJ. Radiation driven planar foil instability and mix experiments at the AWE HELEN laser. *Laser and Particle Beams* 1990; **8**:51–71.
20. Nie X, Qian Y-H, Doolen GD, Chen S. Lattice Boltzmann simulation of the two-dimensional Rayleigh–Taylor instability. *Physical Review E* 1998; **58**:6861–6864.
21. Tartakovsky AM, Meakin P. A smoothed particle hydrodynamics model for miscible flow in three-dimensional fractures and the two-dimensional Rayleigh–Taylor instability. *Journal of Computational Physics* 2005; **207**: 610–624.
22. He X, Zhang R, Chen S, Doolen GD. On the three-dimensional Rayleigh–Taylor instability. *Physics of Fluids* 1999; **11**:1143–1152.
23. Goncharov VN. Analytical model of nonlinear, single-mode, classical Rayleigh–Taylor instability at arbitrary Atwood numbers. *Physical Review Letters* 2002; **88**:134504.
24. Ramaprabhu P, Dimonte G, Young Y-N, Calder AC, Fryxell B. Limits of the potential flow approach to the single-mode Rayleigh–Taylor problem. *Physical Review E* 2006; **74**:066308.
25. Rowlinson JS, Widom B. *Molecular Theory of Capillarity*. Oxford University Press: Oxford, 1982.
26. He X, Chen S, Zhang R. A lattice Boltzmann scheme for incompressible multiphase flow and its application in simulation of Rayleigh–Taylor instability. *Journal of Computational Physics* 1999; **152**:642–663.
27. McCracken M, Abraham J. Multiple-relaxation-time lattice Boltzmann model for multiphase flows. *Physical Review E* 2005; **71**:036701.
28. Premnath KN, Abraham J. Lattice Boltzmann model for axisymmetric multiphase flows. *Physical Review E* 2005; **71**:056706.
29. Lucy LB. A numerical approach to the testing of the fission hypothesis. *Astronomical Journal* 1977; **82**:1013–1024.
30. Kim O, Hoover WG, Hoover CG. Smooth-particle boundary conditions. *Physical Review E* 2003; **68**:017701.
31. Hoover WG, Hoover CG. Smooth-particle phase stability with generalized density-dependent potentials. *Physical Review E* 2006; **73**:016702.
32. Dzwinel W, Alda W, Pogoda M, Yuen DA. Turbulent mixing in the microscale: a 2D molecular dynamics simulation. *Physica D* 2000; **137**:157–171.
33. Kadau K, Germann TC, Hadjiconstantinou NG, Lomdahl PS, Dimonte G, Holian BL, Alder BJ. Nanohydrodynamics simulations: an atomistic view of the Rayleigh–Taylor instability. *Proceedings of the National Academy of Sciences of the United States of America* 2004; **101**:5851–5855.
34. Revenga M, Zuniga I, Espanol P. Boundary conditions in dissipative particle dynamics. *Computer Physics Communications* 1999; **121–122**:309–311.
35. Read KI. Experimental investigation of turbulent mixing by Rayleigh–Taylor instability. *Physica D* 1984; **12**: 45–58.
36. Youngs DL. Modelling turbulent mixing by Rayleigh–Taylor instability. *Physica D* 1989; **37**:270–287.
37. Davies RM, Taylor GI. The mechanics of large bubbles rising through extended liquids and through liquids in tubes. *Proceedings of the Royal Society of London, Series A* 1950; **200**:375–390.

DOI: 10.1002/fld